Fuel 226 (2018) 508–515

Contents lists available at ScienceDirect

Fuel

journal homepage: www.elsevier.com/locate/fuel

Full Length Article

Thermal inertia effects of the structural elements in heat losses during the charcoal production in brick kilns

Jaime Daniel Bustos-Vanegas, Marcio Arêdes Martins*, Angélica de Cassia Oliveira Carneiro, Arthur Gomes Freitas, Ruben Christian Barbosa

Universidade Federal de Viçosa, Viçosa 36570-900, Brazil

ARTICLE INFO

Keywords:
Biomass
Heat transfer
Modeling
Simulation
CFD

ABSTRACT

Brazil is the largest producer of charcoal from planted forests with 5.5 million tons in 2016. The Brazilian steel industry consumes 85% of the national production of charcoal from eucalyptus. The walls and floor of industrial brick kilns are built using isolation materials that minimize heat losses during the wood carbonization stage. However, the thermal inertia of these components represents additional heat that must be removed during the charcoal cooling stage, as reflected in the extended process time. This study aims to evaluate the effect of the thermal inertia of the kiln structural elements for the charcoal production. A CFD (Computational Fluid Dynamics) analysis was performed to simulate the heating and cooling of the system composed of wood, carbonization gases, brick walls and floor. A typical industrial kiln with capacity of 700 m^3 was modeled and validated using a set of experimental measurements of temperatures during a 4-day carbonization stage with final temperature of 400 °C and an 8 day cooling stage. The temperature profile in the walls was linear, corresponding to a pseudo-steady state, where the thermal load increases with the pyrolysis time. The heat transfer at the floor is extensive; therefore, the adiabatic boundary condition cannot be imposed at the wood bed–floor interface. Our findings provide important information for the improvements in the kiln operation and allow establishment of consistent initial conditions of temperature and heat flux for kinetics models for charcoal cooling in kilns.

1. Introduction

Brazil is the largest producer and consumer of charcoal from planted forests, with production reaching 5.5 million tons in 2016 [1]. In terms of Brazil's market share, 85% of the production is destined for industrial use, mainly as a bio-reducer of iron ore in the pig iron and steel industries [1]. Charcoal is a renewable product with advantages over coal because of its higher carbon content, which contributes to the reduction of CO_2 emissions. However, the implicit production cost of charcoal is a limiting factor of its use.

In the current scenario, where global warming is a reality, production systems should be designed with consideration of not only economic gain but also, reducing environmental impacts. In the charcoal process, efforts are focused on the reduction of the emissions of pollutant gases via burning the outlet stream and extraction of the released energy [2,3] and on the process optimization, via reduction of the cooling time.

Charcoal production is based on a thermochemical process known as slow pyrolysis. The quality of the charcoal is a function of the wood quality and carbonization rate. The process occurs in four stages governed by the temperature: wood drying, up to 110 °C; roasting, up to 250 °C; carbonization, up to 350 °C; and carbon fixation, up to 450 °C [4,5]. After the last stage, the charcoal mass into the kiln should be cooled prior the discharge. The carbonization time in typical rectangular kilns, that varies between 190 and 700 m^3 of capacity is approximately 4 days, with the cooling time via natural convection of 9 and 14 days, respectively.

The carbonization process is performed in brick kilns. The bricks have insulating characteristics adequate for the carbonization phase, but unfavorable for the cooling, resulting in a long process time and therefore low productivity. Cooling the charcoal bed involves cooling the inner gases, the walls and even the floor of the kiln, which is usually composed of compacted clay. The thermal properties of those structural elements affect the overall heat transfer and needs to be well known.

Artificial cooling systems via forced heat convection have been developed by companies in an attempt to reduce the cooling time and consequently to increase the productivity [6,7]. Some prototypes using evaporative cooling have also been tested [8], although without

* Corresponding author.
E-mail address: aredes@ufv.br (M.A. Martins).

https://doi.org/10.1016/j.fuel.2018.04.024
Received 30 November 2017; Received in revised form 10 February 2018; Accepted 4 April 2018

Nomenclature

a	absorption coefficient
l	characteristic length, m
γ	charcoal emissivity
C	constants in the turbulence model
S	Coordinate along the path of radiation
ρ	density kg/m^3
ε	dissipation rate of the turbulent kinetic energy, m^2/s^2
L_c	dome height, m
μ	dynamic viscosity, Pa s
σ_ε	equivalent Prandtl number for dissipation of the turbulent kinetic energy
σ_k	equivalent Prandtl number for the turbulent kinetic energy
β	expansion coefficient, K^{-1}
h_{ext}	external heat transfer coefficient by convection, W/m^2 K
$\vec{V}$	fluid velocity [(u, v, w)], m/s
Gr	Grashof number
g	gravity, m/s^2
A_s	interfacial area, m^{-1}
h_i	interfacial heat transfer coefficient, W/m^2 K
δ_{ij}	Kronecker delta
Φ	phase function for scattering
d_p	pore diameter, m
φ	porosity
Pr	Prandtl number
i	radiation intensity, W/m^2
Pk	rate production of the turbulent kinetic energy, Pa/s
Ra	Rayleigh number
τ	Reynolds stress tensor
σ_s	scattering coefficient
ω	solid angle
C_p	Specific heat, J/kg K
σ	Stefan-Boltzmann constant
T	Temperature, K
k	Thermal conductivity, W/m K
t	time, s
k^T	turbulent kinetic energy, m^2/s^2
L_w	wall height, m
C_{pw}	wall specific heat, J/kg K
T_w	wall temperature, K
λ	wavelength

Subscripts

b	Floor
f	Fluid phase
s	Solid phase
t	turbulence
w	Wall
ef-s	effective thermal conductivity
surf	external surface
s-i	Internal surface

thorough knowledge of the carbonization and cooling kinetics, thus limiting their implementation on an industrial scale.

Modeling and simulation are tools for use in analysis, design and project optimization. Some previous research focused on modeling the process of charcoal cooling and charcoal carbonization [8–10] with adoption of simplifications that sometimes do not consider physical phenomena of importance, e.g., time-dependent boundary conditions. Computational fluid dynamics (CFD) allows the evaluation of different scenarios and configurations of cooling and carbonization systems in simulated prototypes, saving both costs and time of experimentation.

This study is the first report in the literature of a mathematical model for simulation the carbonization in a rectangular brick kiln. The model was used to investigate the thermal inertia of the structural components and to provide information for formulation of mathematical models that include the heat transfer during the charcoal cooling.

2. Methodology

2.1. Experimental setup

The carbonization kiln under study corresponds to the industrial model 390 from Vallourec Florestal, with wood load capacity of 700 m^3, internal dimensions of 32 m in length, 4 m in width, 4 m in height, with a1.2 m high dome (Fig. 1). The walls are built with 0.24-m thick clay brick and doors at each end are constructed of concrete with a thin metal structure. Four chambers located below the kiln provide the energy required for ignition and for starting the pyrolysis. The ignition chambers are four structures located just below the floor surface (Fig. 1B) and equidistant throughout the kiln. In this chambers, wood is burnt at the beginning of the process (first 5 h of the carbonization stage). The gases resulting from this combustion process are conducted along the kiln by a channel located just below the floor (Fig. 1D). These hot gases circulate the bed of wood providing the energy for starting the pyrolysis. The two energy sources at the base of the wood bed (Fig. 1C) represents the energy provided for the combustion gases, which are responsible for the natural convection flow into the porous section and the gas head space over the bed. Its implementation into the model will be described further on.

The carbonization stage takes 4 days with a final temperature of 400 °C. The further cooling stage lasts for 8 days in natural convection condition with a final temperature of 50 °C. The carbonization gases flow through a duct to a central burner.

Three production cycles were monitored via a data acquisition system consisting of 17 J-type shielded thermocouples 4 AWG, three data acquisition modules (ICP CON 7018) and one interface module (ICP CON 7520) connected to a computer. At 1 m high, the thermocouples recorded the average of 11 measuring points of temperature of the inner wall face during the carbonization and cooling stages. At 3.8 m high, the average of 6 measuring points of temperature of the inner wall face were registered. The average temperatures recorded during the three cycles were used to validate the proposed model.

2.2. Model and simulation

The carbonization cycle was modeled to quantify the thermal effects of the thermo-chemical conversion of the wood bed to charcoal. It is important to remark that the focus of this work was not the modeling of pyrolysis reactions. Therefore, the overall heat generated by the wood drying and subsequent pyrolysis was modeled as an energy source in the heat transfer governing equations. This source was calculated based on a thermal balance and adjusted for typical values of reaction heat of pyrolysis in literature. A typical carbonization cycle of 12 days (4 days for the carbonization stage and 8 days for the cooling stage) was modeled and simulated with the CFD technique using ANSYS CFX v11.0 software.

2.2.1. Physical model

The computational domain is defined by the kiln brick wall, the clay floor and the inner porous material (Fig. 1). Because the length of the kiln is significantly greater than its width, the heat transfer to the external environment occurs mainly in the cross-section. Thus, a two-dimensional approach can be performed, creating two solid subdomains

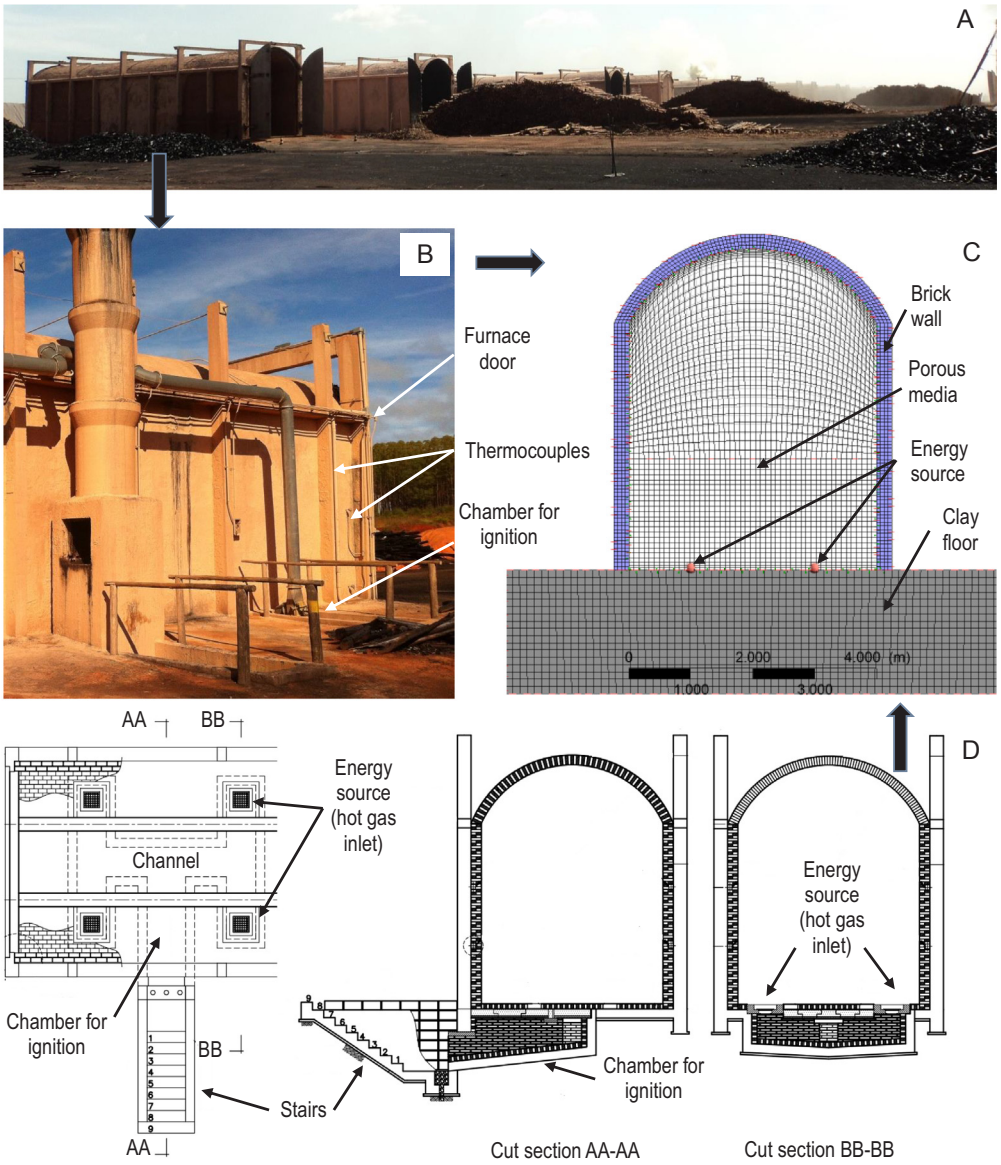

Fig. 1. Typical Brazilian charcoal plant (A). Brick kiln with thermometry system and ignition chamber (B). Computational domain detailing a two-dimensional approach for the kiln cross-section (C). Top and side view of brick kiln showing detail of combustion chamber and hot gas inlet (D).

(walls and floor), and one porous domain to represent the wood and charcoal inside the kiln (Fig. 1C). The porous medium corresponds to the wooden bed with logs positioned horizontally. Initially, the bed occupies the total space of the kiln, and as the pyrolysis progresses, the wood degrades and shrinks. The bed height was then defined as a function dependent on the process time, decreasing up to 1.8 m at the end of the carbonization stage (4th day) and remaining constant during the cooling.

In order to investigate the heat diffusion effects through the floor, this subdomain was extended up to 4 m depth and 2 m on each side, as depicted in Fig. 1.

The computational domain was discretized for each subdomain, which allows a set of meshes with good orthogonality. After a previous spatial and temporal convergence testing, a mesh of 13,740 elements (8820 for the porous subdomain, 888 for the wall subdomain and 4032 for the floor subdomain) and a time step of 60 min were chosen. A mesh refinement was applied at the bed-walls and bed-floor interfaces to improve the heat flux conservation and temperature continuity.

2.2.2. *Governing equations*

Because the aim of this research was to understand the heat transfer and its inertia in the structural components of the kiln, the following assumption were adopted:

a) The intergranular gas inside the kiln is an ideal mixture of CO_2 and N_2.
b) Buoyant force modeled using the Boussinesq approach.
c) Low-Mach number: density changes only associated with temperature variations.
d) Charcoal bed is considered as an isotropic porous medium in the condition of local thermal non-equilibrium.
e) Thermal radiation intensity is isotropic.

The governing equations of the transient model were based on the continuity, momentum and energy equations. For the porous medium:

$$\varphi\frac{\partial\rho_f}{\partial t} + \nabla\cdot(\rho_f\vec{v}) = 0 \quad (1)$$

$$\frac{\partial(\rho_f \vec{v})}{\partial t} + \frac{1}{\varphi}\nabla\cdot(\rho_f \vec{v}\vec{v}) = -\varphi\nabla P + \mu\nabla^2\vec{v} + \rho_f \vec{g} - \frac{\varphi\mu}{K}\vec{v} - \frac{\varphi\rho_f C_E}{\sqrt{K}}\vec{v}\vec{v} \quad (2)$$

$$(1-\varphi)(\rho C_p)_s \frac{\partial T_s}{\partial t} = (1-\varphi)\nabla\cdot(k_{ef-s}\nabla T_s) + (1-\varphi)q_s''' + h_i A_s(T_f - T_s) \quad (3)$$

$$\varphi C_{pf}\frac{\partial(\rho_f T_f)}{\partial t} + \nabla\cdot(C_{pf}\rho_f T_f \vec{v}) = \varphi\nabla\cdot(k_f\nabla T_f) - h_i A_s(T_f - T_s) \quad (4)$$

Terms on the left hand side in Eqs. (14) represent transient and advective transport. The last two terms of Eq. (2) correspond to the resistive force terms and represent the viscous and drag forces resulting from the interaction between the solid and fluid phases in the porous medium. These two terms were adjusted by experimental measurements of pressure drop, where a quadratic relationship to the true velocity was observed (Table 1). The term associated with the gravity vector in Eq. (2) represents the buoyant force due to the gas density changing with temperature.

During the pyrolysis, heat generation increases and is transferred into the porous bed, creates temperature gradients that promote the gas flow inside the kiln. In the porous media, the flow becomes turbulent when $Re > 280$ [11]. In order to account for turbulence fluctuations, Eqs. (14) were modified to a time-averaged form (Reynolds-Averaged Navier-Stokes equations), where the Reynolds stress tensor (τ) in Eq. (2) is modeled using an eddy viscosity, μ_t:

$$\nabla\cdot\tau = \nabla\cdot(-\rho_f \vec{v}\vec{v}) \quad (5)$$

$$-\vec{v}'\vec{v}' = \mu_t\left(\frac{\partial\vec{v_i}}{\partial x_j} + \frac{\partial\vec{v_j}}{\partial x_i}\right) - \frac{2}{3}\delta_{ij}k \quad (6)$$

where δ_{ij} is the Kronecker delta and k is the kinetic energy of the velocity fluctuations. The terms on the right-hand side of Eq. (6) represent the Reynolds shear and normal stresses. To close the system of the governing equations, the Reynolds stress was modeled by the k-ε model [12,13]:

$$\mu_t = C_\mu\rho_f\frac{k^{T^2}}{\varepsilon} \quad (7)$$

$$\frac{\partial(\rho_f k^T)}{\partial t} + \nabla\cdot(\rho_f \vec{v} k^T) = \nabla\cdot\left[\left(\mu + \frac{\mu_t}{\sigma_k}\right)\nabla k^T\right] + P_k - \rho_f\varepsilon \quad (8)$$

$$\frac{\partial(\rho_f\varepsilon)}{\partial t} + \nabla\cdot(\rho_f\vec{v}\varepsilon) = \nabla\cdot\left[\left(\mu + \frac{\mu_t}{\sigma_\varepsilon}\right)\nabla\varepsilon\right] + \frac{\varepsilon}{k^T}(C_{\varepsilon 1}P_k - C_{\varepsilon 2}P_\varepsilon) \quad (9)$$

$$P_k = \mu_t\nabla\vec{v}(\nabla\vec{v} + \nabla\vec{v}^T) - \frac{2}{3}(\nabla\vec{v})(3\mu_t\nabla\vec{v} + \rho_f k^T) \quad (10)$$

where k^T is the turbulent kinetic energy, ε is the rate of dissipation and σ_k, σ_ε, $C_{\varepsilon 1}$ and $C_{\varepsilon 2}$ are closure parameters with values of 1.0, 1.3, 1.44 and 1.92 respectively [12,13].

Eqs. (3) and (4) describe the energy transport in the solid and fluid phases of porous medium, respectively. The source term q''' in the solid phase represents the energy supplied for the ignition and the consequent energy released during the partial oxidation reactions (reaction heat of pyrolysis). In the pyrolysis reaction, the main components of the wood (hemicellulose, cellulose and lignin) are degraded at different rates following an Arrhenius type reaction kinetic [14]. Other authors proposed an alternative and complementary approach in which the degradation rate varies as a function of the reaction product: intermediate solid, char, tar or gas [15–17].

The reaction heat of pyrolysis, varies in a wide range. Dougaard and Brown [18] reported values varying from 0.78 to 1.64 MJ kg^{-1} depending on the type of biomass source. A value of 0.93 MJ kg^{-1} was set during the carbonization stage (four days) in order to run the simulations. This term was implemented in CFX acting in the two-point energy sources (shown in Fig. 1C) during the first five hours of the process. For the rest of time of carbonization stage, the source term was set to act on the whole porous subdomain. After, for the cooling stage, this value was set to zero. Table 1 presents the model parameters used in the simulation.

The heat transfer by the gas flow through the porous matrix is proportional to the interfacial heat transfer coefficient h_i. These term was assumed to act inside the porous bed locally and it depends on the gas properties, characteristic length of particles (l) and Nusselt number (Nu). This dimensionless number relates the contribution of the convective and conductive mechanisms in the heat transfer phenomena at the fluid-solid interphase. The coupling term (h_i) appears in the two energy equations (Eqs. (3) and (4) accompanying the interstitial heat exchange specific area (A_s):

$$h_i = k_f\frac{Nu}{l} \quad (11)$$

The interfacial gas flow, driven by the buoyancy force, circulate the porous bed toward the heat space. In this free flow region, which expands as the porous bed shrinks, the gas reaches a higher velocity, resulting in larger Reynolds numbers and increasing convective heat transfer at the bed surface. Because of this, the carbonization front runs from top to bottom of the bed.

Radiation between particles is considered in Eq. (3) within the diffusive term, in which the effective heat transfer coefficient $k_{ef\text{-}s}$ quantifies the conduction and radiation phenomena [19]:

$$k_{ef-s} = k_c + k_{rad} \quad (12)$$

$$k_{rad} = 4\varphi\sigma\gamma d_p T_s^3 \quad (13)$$

where σ is the Stefan-Boltzmann constant, ψ is the charcoal emissivity and d_p is the average diameter of the charcoal pores. Energy traveling as

Table 1
Model parameters.

Wall (brick fireclay) [22]	Value
c_{pw} [J kg^{-1} K^{-1}]	960
k_w [W m^{-1} K^{-1}]	1,0
ρ_w [kg m^{-3}]	2645
Clay floor [22]	
c_{pb} [J kg^{-1} K^{-1}]	880
k_b [W m^{-1} K^{-1}]	1,29
ρ_b [kg m^{-3}]	1450
Porous media (fluid phase) [12]	
CO_2 thermophysical properties	Ansys CFX database
N_2 thermophysical properties	Ansys CFX database
Porous media (solid phase) [6,17,22]	
c_p *wood* [J kg^{-1} K^{-1}]	2385
k *wood* [W m^{-1} K^{-1}]	0,19
ρ *wood* [kg m^{-3}]	540
c_p *charcoal* [J kg^{-1} K^{-1}]	1017
k *charcoal* [W m^{-1} K^{-1}]	0,03
ρ *charcoal* [kg m^{-3}]	345
l [m]	0.13
ψ	0,9
d_{pore} [μm]	350
Porous media [6,18]	
ε	0,6
A_s [m^{-2}]	65
Nu	$2 + (1.1\,Pr^{0.33}\,Re^{0.6})$
$\Delta P/l$ [Pa m^{-1}]	$24\,V + 343\,V^2$
q'''[W m^{-3}]	1185
Carbonization time [h]	96
Cooling time [h]	192

radiation through the interstitial fluid can be modeled using an additional transfer equation for the porous domain, where the change in intensity is a balance among emission, absorption and scattering [20,21]:

$$\frac{\partial i_\lambda}{\partial S} = a_\lambda i_{\lambda b}(S) - a_\lambda i_\lambda(S) - \sigma_{s\lambda} i_\lambda(S) + \frac{\sigma_{s\lambda}}{4\pi}\int_{\omega_i}^{4\pi} i_\lambda(S,\omega_i)\phi(\lambda,\omega,\omega_i)d\omega_i \quad (14)$$

The first term on the right side of Eq. (14) represents the gain by emission, followed by the loss terms of absorption and scattering. The last term represents the gain by scattering. The radiation emitted by the wood bed (under carbonization conditions) interacts with the fluid region above it and with the inner surfaces of the kiln. This is known as limit diffusion, because radiant energy is dispersed in all directions. The radiation model P1 was adopted to account for the radiant heat flux, because the medium inside the kiln is optically dense and approaches the limit diffusion condition. The P1 model simplifies the radiative transfer equation and reduces the required computational effort.

The walls and floor are defined as impermeable with average properties. For these domains, a transport equation is only required for energy, in which the diffusive mechanism is governing:

$$C_{pw}\rho_w \frac{\partial T_w}{\partial t} = k_w \nabla^2 T_w \quad (15)$$

$$C_{pb}\rho_b \frac{\partial T_b}{\partial t} = k_b \nabla^2 T_b \quad (16)$$

2.2.3. Boundary conditions and interfaces

The hydrodynamic conditions at the bed-wall and bed-floor interfaces are no-slip, zero speed and thermal energy conservation along the normal direction:

$$-\left[k_b \frac{\partial T_b}{\partial n}\right]_{base} = \left[-k_{ef-s}\frac{\partial T_s}{\partial n} - k_f \frac{\partial T_f}{\partial n}\right]_{porous} \quad (17)$$

$$-\left[k_w \frac{\partial T_w}{\partial n}\right]_{wall} = \left[-k_{ef-s}\frac{\partial T_s}{\partial n} - k_f \frac{\partial T_f}{\partial n}\right]_{porous} \quad (18)$$

$$h_i[T_{s-i,t} - T_f] = k_w \frac{\partial T_{s-i,t}}{\partial x} \quad (19)$$

Eqs. (17) and (18) model the heat flux at the bed-wall and bed-floor interfaces. Eq. (19) responds by the heat flux between the head space inside the kiln and the inner surface of the walls.

For the carbonization stage, the boundary conditions were established as the following: on the floor, at a depth of 2 m, an adiabatic boundary condition is set; in the symmetry planes, normal gradients are set to zero for all quantities; on the external wall surface, a convective boundary condition is established with outside temperature set to 25 °C:

$$h_{ext}[T_{surf,t} - T_\infty] = k_w \frac{\partial T_{surf,t}}{\partial x} \quad (20)$$

The convection heat transfer coefficient was calculated considering an average air velocity of 4.5 m/s and outside temperature of 25 °C. Following the experimental approach proposed by [9], an approximation was made depending on the height of the kiln:

Lateral wall, for $0.3 < Pr_{air} < 100$ and $10^10 < Ra < 10^13$:

$$h_{ext} = [0.138\frac{k_{air}}{L_w} Gr^{0.36}(Pr_{air}^{0.175} - 0.55)][1 + (2.237 fv_{air})] \quad (21)$$

Dome, for $Ra > 10^8$:

$$h_{ext} = 0.10\frac{k_{air}}{L_c} Ra^{1/3}[1 + (2.237 fv_{air})] \quad (22)$$

Where f is a correction factor that depends on the temperature difference between external surface and air [9]: $f = 0{,}229$ for $\Delta T = 8.33$ °C $f = 0{,}200$ for $\Delta T = 13.89$ °C $f = 0{,}171$ for $\Delta T = 27.78$ °C $f = 0{,}150$ for $\Delta T = 55.56$ °C $f = 0{,}121$ for $\Delta T = 111.11$ °C

As initial conditions for carbonization stages, all temperatures were set to 25 °C. For the cooling stage, the boundary conditions were maintained, except for the adiabatic boundary condition in the floor, which was modified to a depth of 4 m. The simulated conditions at the end of the carbonization stage were used as the initial conditions for the cooling stage, by switching to zero the heat source term in the energy equation (Eq. (3)).

The simulation time was set to 96 h (4 days) for the carbonization stage and 192 h (8 days) for the cooling stage. The first-order backward Euler and high-resolution discretization schemes were used for the transient and advective terms, respectively. The residual target was set to RMSE $< 10^{-6}$.

3. Results and discussion

3.1. Model validation

Average of six experimental measurements points of temperature at height of 3.8 m and 11 measurements points of temperature at 1 m height on the inner surface of the wall were compared with the simulation data (Fig. 2). The CFD predictions are found to be in good agreement with the experimental data, with R^2 of 92% and 95% for the carbonization and cooling stages, respectively. In the highest position (Fig. 2A), as a consequence of the buoyancy forces, a rapid increase in temperature is observed due to the flow of hot gases toward the head space. The internal wall temperature reached almost 300 °C at the end of carbonization stage, and it is a characteristic temperature used by charcoal producers to monitor the behavior of pyrolysis inside the kiln.

3.2. Simulation

During the carbonization stage (Fig. 3), the advance of the carbonization front can be observed from the top to the bottom of the kiln. By having a much lower density compared to wood, stagnant gases at the top of the bed are heated rapidly, creating a convective flow that promote the carbonization front. The simulated Reynolds number varies between 250 for the porous bed and 8800 for the head space, a

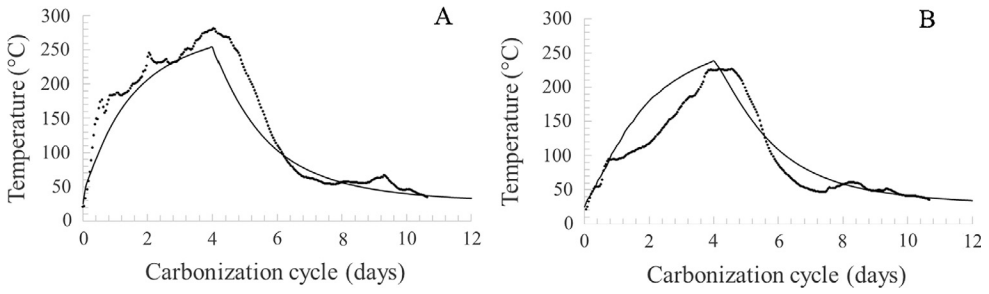

Fig. 2. Experimental (dotted line) and simulated (black line) temperature at the internal surface of the wall at a height of 3.8 m (A) and at a height of 1 m (B) during carbonization cycle. Four days for carbonization stage. Eight days for cooling stage.

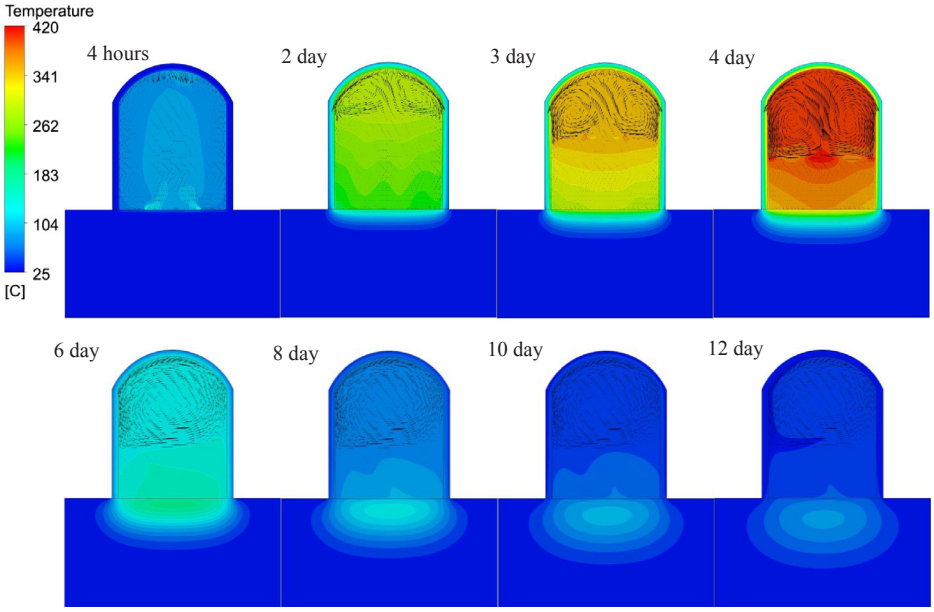

Fig. 3. Temperature distribution of the fluid phase of the charcoal bed, walls and floor during the whole carbonization cycle. The arrows indicate the gas flow pattern at the head space.

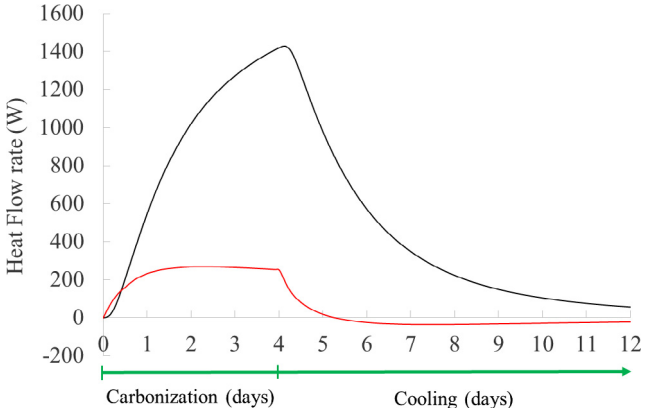

Fig. 4. Heat flow rate at walls (black line) and floor (red line) during the carbonization cycle. (For interpretation of the references to colour in this figure legend, the reader is referred to the web version of this article.)

condition that justifies the use of a turbulence model. Similarly, during the cooling, the gas phase in the head space releases heat rapidly and therefore decreases its temperature at higher rates than the bed. This phenomenon has been observed in the industry during the opening of the kilns, where apparently cold kilns can undergo combustion breakouts when the air comes into contact with still hot pieces of charcoal lies inside the bed.

The heat diffusion through the floor can also be observed in Fig. 3. During the carbonization stage, the heat diffuses from the heated bed to the floor. The diffusion in the depths of the floor continues during the cooling stage, and a zero-temperature gradient can be observed by the boundary condition imposed (4 m depth and 2 m on each side). After the fifth day of processing (first day of cooling), the temperature at the floor is found to exceed the temperature of the bed above the kiln (i.e. interface). This condition results in a reverse heat flux at floor interface, in which the bed begins to absorb energy from the floor (dotted-line, Fig. 4), making it difficult to cool down the bed.

The heat flow through the walls is faster than the heat flow at the bed-floor interface (Fig. 4). The walls exchange heat with the environment via convection and radiation, reaching a maximum value of 1427 W at the end of the carbonization stage. At the beginning of the cooling (during the first two days), a higher heat rate can also be observed. Soon after, the heat rate begins to decline exponentially, reflecting a long cooling time. Sixty hours after the process start (the second day of carbonization), the heat flux at the floor interface is 260 W, and presented a tendency to remain stable until the end of the carbonization stage. On the second day of cooling (approximately 32 h), the heat rate reverses its direction and the bed begins to absorb heat from the floor. The exposed phenomenon highlights the importance of not considering the floor as adiabatic and address new possibilities for different approaches to understand the cooling problem and its further

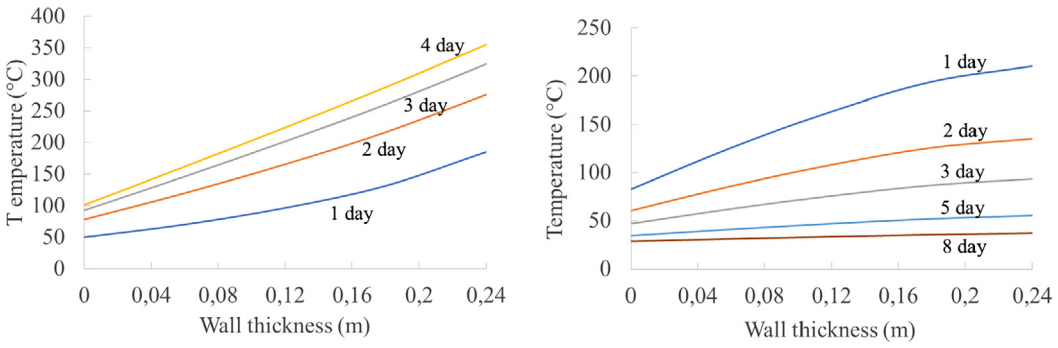

Fig. 5. Temperature distribution into the wall during the carbonization (A) and cooling stages (B) at 0.8 m high.

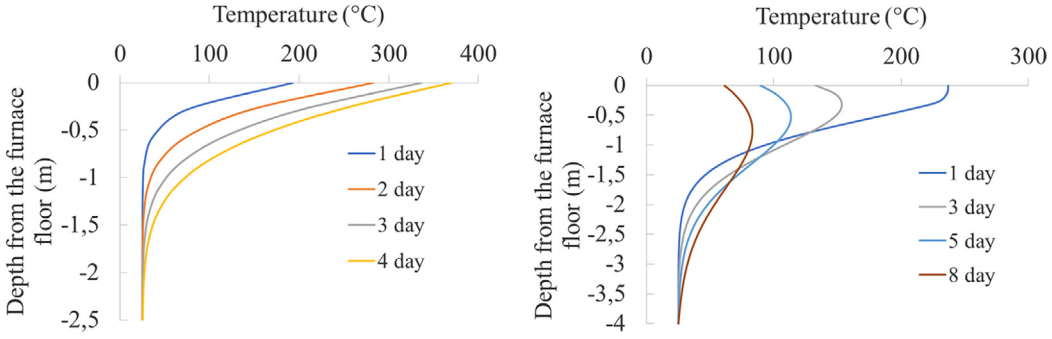

Fig. 6. Temperature distribution into the floor during the carbonization stage (A) and during the cooling stage (B).

optimization.

The integration of the heat flow rate function shown in Fig. 4 enables estimation of the heat losses during the process. During the carbonization stage, 302.8 MJ are lost through the walls and 69.9 MJ are lost through the floor. These values represent 46.8% of the total energy required in the process (794.8 MJ). Current research in the field of material science evaluating insulation characteristics in bricks [22–24] could be applied in the charcoal industry. Materials with lower thermal conductivity would minimize losses during carbonization but could extend the cooling time even further.

The temperature distribution at the wall thickness during the carbonization and cooling stages is shown in Fig. 5, at 0.8 m high. The linear profile corresponds to pseudo steady state heat conduction, where the thermal load increase with the pyrolysis time (Fig. 5A). This behavior enables modeling of the wall domain with fewer mesh elements. Additionally, the brick walls can be modeled even without a physical domain, using the thermal resistance approach [22]. This approach could result in a lower CPU running time.

For a one-dimensional plane wall, Fourier's law establishes that the heat flux is proportional to the temperature gradient. After the second day of cooling (Fig. 5B), the temperature gradient decreases considerably, relying on a low heat transfer rate.

Two inlets at the floor provide the heat to start the wood pyrolysis at the beginning of carbonization process. A controlled combustion occurs from the inlet chambers, and then, the process become self-sustaining as the pyrolysis reaction occurs. The floor surface is heated rapidly during the first day when the chambers are active. During the carbonization stage, heat diffusion through the floor starts from the surface and reaches a depth of almost 2 m, where an adiabatic boundary condition can be correctly established (Fig. 6A).

During the cooling stage, heat diffusion through the floor continues and the adiabatic boundary condition had to be moved to the depth of 4 m (Fig. 6B). After the first day of cooling, the floor's temperature is found to exceed the temperature of the interface (Fig. 6B), thereby inverting the heat flux, as observed in Fig. 4. Therefore, the use of an insulation layer at the floor will contribute to a more effective conversion from wood to charcoal, since the heat loss though the kiln floor will be no longer significant. Moreover, with an insulation layer, the cooling stage will be also improved since no heat will be transferred from the clay floor to charcoal.

4. Conclusions

Computational fluid dynamics was presented as a reliable tool for the modeling and simulation of the thermal phenomena involved in the pyrolysis and cooling stages in the production of charcoal in industrial scale kilns.

The thermal inertia of the structural elements of a brick kiln was characterized by determining the temperature profile and heat flux through the walls and floor during the carbonization and cooling stage. The temperature profile in the brick walls showed a pseudo-steady state behavior that allows modeling this subdomain using the thermal resistance method. This approach can reduce computational time in simulations using the CFD method.

The analysis of the heat flux through the structural elements of the kiln allows the quantification of the heat losses in each stage of the process. The bed-floor interface cannot be considered adiabatic. The floor can be only considered as adiabatic at 2 m depth during the carbonization stage and at 4 m depth during the cooling. The time when the charcoal bed begins to absorb heat from the floor is crucial for the design of carbonization and cooling systems, evaluating different materials and configurations for their optimization.

The simplified model presents an adequate prediction of temperature distribution at walls, floor and porous material. These temperature fields can be used as the initial conditions in the computational model formulation of the cooling process of brick kilns, enabling the simulated conditions to approach the real conditions.

Acknowledgments

The authors thank Brazilian funding agencies CAPES and CNPq, and the Department of Agricultural Engineering of Universidade Federal de Viçosa for providing research funding and scholarship.

References

[1] Empresa de Pesquisa Energética. Balanço Energético Nacional; 2017: 70–1.
[2] Pereira EG, Martins MA, Pecenka R, de Carneiro A. C. Pyrolysis gases burners: Sustainability for integrated production of charcoal, heat and electricity. Renew Sustain Energy Rev 2016;75. 592–00.
[3] Coelho M. Desenvolvimento de metodologia para o dimensionamento de câmaras de combustão para gases oriundos do processo de carbonização de madeira [dissertation]. Universidade Federal de Viçosa; 2013.
[4] Peláez-samaniego MR, Garcia-Perez M, Cortez LB, Rosillo-Calle F, Mesa J. Improvements of Brazilian carbonization industry as part of the creation of a global biomass economy. Renew Sustain Energy Rev 2008;12:1063–86.
[5] Carneiro Ade CO, Vital BR, Oliveira AC, Pereira BL. Pirólise lenta da madeira para produção de carvão vegetal. In: Santos F, Colodette J, Queiroz J, editors. Bioenergia e Biorrefinaria: cana de açúcar e espécies florestais. Viçosa: UFV; 2013. p. 429–58.
[6] Santos I. Resfriamento artificial de carvão vegetal em fornos de alvenaria [dissertation]. Universidade Federal de Viçosa; 2013.
[7] Oliveira AC, Carneiro A de C, Barcellos DC, Rodriguez AV, Amaral BM, Pereira BL. Resfriamento artificial em fornos retangulares para a produção de carvão vegetal. 2015;39(4):769–78. [Portuguese].
[8] Reis H. Resfriamento de fornos de carbonização por injeção de vapor de água [dissertation]. Universidade Federal de Viçosa; 2009.
[9] França GAC, Campos MB. Análise teórica e experimental do resfriamento de carvão vegetal em forno rectangular. IV Encontro de Energia no Meio Rural; 2002 Oct 28–31; Campinas (SP), Brazil.
[10] Centro de Gestão e Estudos Estratégicos. Metodologia de estudo e analise de escoamento de gases com transferência de calor por médio de simulação computacional em CFD para otimização do processo de carbonização da madeira em tecnologia DPC. Plano siderurgia MDIC: Modernização de produção de carvão vegetal; 2014.
[11] Lesage F, Midoux N, Lafiti MA. New local measurements of hydrodynamics in porous media. Exp Fluids 2004;37:257–62.
[12] Saito M, de Lemos M. A macroscopic two-energy equation model for turbulent flow and heat transfer in highly porous media. Int J Heat Mass Transf 2010;53:2424–33.
[13] Pedras M, de Lemos M. Computation of turbulent flow in porous media using a low Reynolds k-ε model and an infinite array of transversally-displaced elliptic rods.

Numer Heat Transfer, Part A 2003;43(6). 585-02.
[14] Mehrabian R, Zahirovic S, Scharler R, Obernberger I, Kleditzsch S, Wirtz S, et al. A CDF model for thermal conversion of thermally thick biomass particles. Fuel Process Technol 2012;95. 96-08.
[15] Park WC, Atreya A, Baum HR. Experimental and theoretical investigation of heat and mass transfer processes during wood pyrolysis. Combust Flame 2010;157:481–94.
[16] Grieco E, Baldi G. Analysis and modelling of wood pyrolysis. Chem Eng Sci 2011;66:650–60.
[17] Pan Y, Kong S. Simulation of biomass particle evolution under pyrolysis conditions using lattice Boltzmann method. Combust Flame 2017;178:21–34.
[18] Daugaard D, Brown R. Enthalpy for pyrolysis for several types of biomass. Energy Fuels 2003;17(4):934–9.
[19] Larfeldt J, Leckner B, Melaaen M. Modelling and measurements of heat transfer in charcoal from pyrolysis of large wood particles. Biomass Bioenergy 2000;18:507–14.
[20] Modest MF. Radiative heat transfer. 2nd ed. California: Academic Press; 2003.
[21] Siegel R, Howell JR. Thermal radiation heat transfer. 3rd ed. Whasington: Hemisphere; 1992.
[22] Bergman TL, Lavine AS, Incropera F, Dewit DP. Fundamentals of heat and mass transfer. 7th ed. New York: John Wiley & Sons; 2011.
[23] Triantafillou TC, Karlos K, Kefalou K, Argyropoulou E. An innovative structural and energy retrofitting system for URM walls using textile reinforced mortars combined with thermal insulation: Mechanical and fire behavior. Constr Build Mater 2017;133:1–13.
[24] Witzany J, Zigler R, Kroftová K. Strengthening of compressed brick masonry walls with carbon composites. Constr Build Mater 2016;112:1066–79.